

Multichannel quantum defect theory for polar molecules

Sergei V. Elfmov,^{*} Dmitrii L. Dorofeev,[†] and Boris A. Zon[‡]*Voronezh State University, 394006 Voronezh, Russia*

(Received 27 August 2013; published 6 February 2014)

Our work is devoted to developing a general approach for nonpenetrating Rydberg states of polar molecules. We propose a method to estimate the accuracy of calculation of their wave functions and quantum defects. Basing on this method we estimate the accuracy of Born-Oppenheimer (BO) and inverse Born-Oppenheimer (IBO) approximations for these states. This estimation enables us to determine the space and energy regions where BO and IBO approximations are valid. It depends on the interplay between l coupling (due to dipole potential of the core) and l uncoupling (due to rotation the core). Next we consider the intermediate region where both BO and IBO are not valid. For this intermediate region we propose a modification of Fano's multichannel quantum defect theory to match BO and IBO wave functions and show that it gives more reliable results. They are demonstrated on the example of SO molecule.

DOI: [10.1103/PhysRevA.89.022507](https://doi.org/10.1103/PhysRevA.89.022507)

PACS number(s): 33.20.-t, 32.80.Ee

I. INTRODUCTION

Comprehensive theoretical description of high-excited atomic and molecular Rydberg states (RSs) is important for interpretation of spectra of astronomical objects [1–3]. In laboratory conditions RSs are obtained up to $n \simeq 300$ [4]. High sensitivity of RSs to external fields and their extremely long-range interactions are attractive for potential technological applications, for example, in quantum computing [5–13]. A special group of RSs is embodied by high- l nonpenetrating ones, where behavior of Rydberg electron can be described by an effective one-electron Hamiltonian. High- l Rydberg spectra are of particular interest because their interpretation allows one to extract properties of the core (atomic or molecular) with high precision [14,15]. Recent identification of many new high- l series [16–20] in atomic spectra allows one to expect appearing precise spectroscopic data on high- l Rydberg series in molecules as well, which makes a challenge for theory.

The motion of electron in a nonpenetrating RS is governed by long-range interactions with the core. The present work is dedicated to developing a general approach to the problem of electron motion in the field of Coulomb potential combined with the field of a freely rotating point dipole. This problem was previously approached from two opposite sides. First, it was considered for the ordinary Born-Oppenheimer (BO) case, when the rotation of the dipole is slow in comparison with the motion of the electron. It was shown to allow an explicit solution due to separation of radial and angular variables [21,22]. Second, the opposite case was considered, referred to as the inverse Born-Oppenheimer (IBO) one, when the dipole rotates much faster than the electron. It became possible to separate radial and angular variables and to get an explicit solution in this case also [23]. Two obtained solutions were used in our previous work [24] for classification and calculation of quantum defects and wave functions for nonpenetrating RSs in polar molecules.

In the present work we suggest a technique applicable to both the above-mentioned limiting cases as well as to the intermediate case, when the rotation of the dipole and the motion of the electron take place at the same time scale. We base it on the multichannel quantum defect theory [25,26] first applied by Fano [27] to a similar problem of RSs in nonpolar molecules. We generalize it by including long-range dipole potential and thus make it applicable to polar molecules as well.

The effect of the core dipole moment on the Rydberg spectrum of real polar molecules was extensively investigated both theoretically and experimentally by the groups of Jungen and Field and other researchers [14,15,28–35]. In particular, in the work [14] the Rydberg spectra of CaF and BaF were calculated for $5 \leq n \leq 12$ and $0 \leq l \leq 6$. However, this calculation was performed entirely in the frame of BO approximation; the effect of the core rotation was not taken into account there. The core rotation was included in the picture in the works [15,28,36], but on the other hand the effect of long-range core dipole potential in IBO region was not consistently accounted for.

In Sec. II of the present work we outline the main formalism. In Sec. II A the effective one-electron Hamiltonian is presented, in Secs. II B and II C the BO and IBO approximations are considered, respectively, in Sec. II D the multichannel quantum defect theory (MQDT) technique is described for matching BO and IBO solutions, and Sec. II E presents an example of choosing proper matching radius and estimating accuracy of the obtained matched wave function. In Sec. III we discuss the results obtained for the model SO molecule. In the Appendix the mathematics of radial Coulomb functions is briefly summarized.

Atomic units are used throughout this work.

II. MAIN FORMALISM

A. Effective Hamiltonian

We take the Hamiltonian of a polar diatomic Rydberg molecule in the following form:

$$H = H^+ + \frac{\mathbf{p}^2}{2} - \frac{1}{r} + \frac{\mathbf{d}\mathbf{r}}{r^3}, \quad (1)$$

^{*}elfimovserg@gmail.com

[†]dmitrii.dorofeev@gmail.com

[‡]zon@niif.vsu.ru

where H^+ relates to the centrifugal energy of the nuclei:

$$H^+ = B\hat{N}^2. \quad (2)$$

\hat{N} is the orbital angular momentum of nuclei,

$$\hat{N} = \hat{\mathbf{J}} - \hat{\mathbf{L}}^+ - \hat{\mathbf{S}}^+ - \hat{\mathbf{I}}, \quad (3)$$

B is the rotational constant, $\hat{\mathbf{J}}$ is the total momentum of the molecule (except the spin of the Rydberg electron), $\hat{\mathbf{L}}^+$ and $\hat{\mathbf{S}}^+$ are the orbital angular momentum and the spin of core electrons, respectively, and $\hat{\mathbf{I}}$ is the orbital angular momentum of the Rydberg electron. The Hund's case (a) for the core is assumed; hence the projection of $\hat{\mathbf{L}}^+ + \hat{\mathbf{S}}^+$ onto the molecular axes is taken to be a good quantum number ω . The electronic state of the core is assumed to be not perturbed by the Rydberg electron, and the constant energy of the core electrons is omitted from the total energy of the molecule throughout the present paper. Vectors \mathbf{r} and \mathbf{p} are the position and the translational momentum of the Rydberg electron, respectively. Spin of the Rydberg electron and vibration of the core are not taken into account.

B. Pure Born-Oppenheimer wave function

If the Rydberg electron spends the most time near the core where the ordinary Born-Oppenheimer approximation is valid, the projection m of \mathbf{l} on the core axis is a good quantum number and the molecular wave function can be taken in the form

$$\Psi_{lm}^{\text{BO}} = R_{lm}^{\text{BO}}(E, r) Z_{lm}^{\text{BO}}(\theta, \varphi, \Omega). \quad (4)$$

The radial function R can be expressed via the Coulomb functions regular at origin and infinity (see the Appendix). The angular function for a nonpenetrating RS of a nonpolar molecule ($d = 0$) can be decomposed as

$$Z_{lm}^{\text{BO}}(\theta, \varphi, \Omega) = \Phi_{M, \Lambda}^J(\Omega) Y_{lm}(\theta, \varphi), \quad (5)$$

where Ω are the Euler angles that specify the spatial orientation of the molecule, Y are ordinary spherical harmonics, θ and φ are the spherical angles of the Rydberg electron in the molecule frame, and M and $\Lambda = \omega + m$ are the projections of \mathbf{J} on the laboratory axis and the molecular one, respectively. The component Φ is related to the rotation of the whole molecule and can be represented in terms of Wigner D functions

$$\Phi_{M, \Lambda}^J(\Omega) = \sqrt{\frac{2J+1}{8\pi^2}} D_{M, \Lambda}^{J*}(\Omega). \quad (6)$$

For a polar molecule ($d \neq 0$) the spherical harmonics Y in (5) should be modified:

$$Z_{lm}^{\text{BO}}(\theta, \varphi, \Omega) = \Phi_{M, \Lambda}^J(\Omega) \tilde{Y}_{lm}(\theta, \varphi), \quad (7)$$

where \tilde{Y} are dipole-spherical functions:

$$-\Delta_{\theta, \varphi} \tilde{Y} + 2d \cos(\theta) \tilde{Y} = \tilde{l}(\tilde{l} + 1) \tilde{Y}, \quad (8)$$

which can be expanded over ordinary spherical harmonics:

$$\tilde{Y}_{lm}(\theta, \varphi) = \sum_{\ell=|m|}^{\infty} a_{\ell}^{(lm)} Y_{\ell m}(\theta, \varphi). \quad (9)$$

The modified eigenvalues \tilde{l} in Eq. (8) and the expansion coefficients $a_{\ell}^{(lm)}$ in Eq. (9) can be readily found by a simple matrix diagonalization procedure [21]. It must be noted that the index l in Eqs. (7) and (9) ceases to be an eigenvalue of the Rydberg electron momentum \mathbf{l} . Here, it is only an enumerator of a modified function \tilde{Y} . The rotational energy of the core in BO approximation is given by the averaging [37]:

$$\begin{aligned} E_{\text{rot}}^+ &= \langle \Psi_{lm}^{\text{BO}} | H^+ | \Psi_{lm}^{\text{BO}} \rangle = B \overline{(\hat{\mathbf{J}} - \hat{\mathbf{L}}^+ - \hat{\mathbf{S}}^+ - \hat{\mathbf{I}})^2} \\ &= B(J(J+1) - 2m\Lambda + \tilde{l}(\tilde{l}+1) - 2\omega^2 + \overline{(\hat{\mathbf{L}}^+ + \hat{\mathbf{S}}^+)^2}). \end{aligned} \quad (10)$$

The last two terms in this expression are constant ones for a given core electronic state; therefore, they will be omitted below. Then the total energy of the molecule in this approximation is given by

$$\begin{aligned} E &= \langle \Psi_{lm}^{\text{BO}} | H | \Psi_{lm}^{\text{BO}} \rangle \\ &= B(J(J+1) - 2\Lambda m + \tilde{l}(\tilde{l}+1)) - \frac{1}{2\nu^2}, \end{aligned} \quad (11)$$

$$\nu = n - \mu^{\text{BO}}, \quad \mu^{\text{BO}} = l - \tilde{l},$$

where n is principal quantum number of the Rydberg electron.

C. Pure inverse Born-Oppenheimer wave function

Oppositely, if the Rydberg electron spends the most time far from the core, then the inverse Born-Oppenheimer approximation is valid [23]. In such a case, the total core momentum $\mathbf{j} = \mathbf{J} - \mathbf{l}$ becomes a good quantum number, and the wave function can be taken in the form

$$\Psi_{lj}^{\text{IBO}} = R_{lj}^{\text{IBO}}(E, r) Z_{lj}^{\text{IBO}}(\theta', \varphi', \Omega), \quad (12)$$

where θ' and φ' are the spherical angles of the Rydberg electron in the laboratory frame. The angular function for a nonpolar molecule is

$$Z_{lj}^{\text{IBO}} = \sum_{l_z, j_z} C_{jj_z l_z}^{JM} \Phi_{j_z, \omega}^j(\Omega) Y_{ll_z}(\theta', \varphi') \quad (13)$$

and for polar molecule

$$\begin{aligned} Z_{lj}^{\text{IBO}} &= \sum_{\ell} a_{\ell}^{(lj)} \sum_{\ell_z, j_z} C_{jj_z \ell_z}^{JM} \Phi_{j_z, \omega}^j(\Omega) Y_{\ell \ell_z}(\theta', \varphi') \\ &= \sum_{\ell} a_{\ell}^{(lj)} \sum_{m'} \sqrt{\frac{2j+1}{2J+1}} C_{j\omega \ell m'}^{J\Lambda} Y_{\ell m'}(\theta, \varphi) \Phi_{M, \Lambda}^J(\Omega), \end{aligned} \quad (14)$$

where again the coefficients $a_{\ell}^{(lj)}$ and the corresponding modified eigenvalues \tilde{l} can be found by a proper diagonalization procedure [Eq. (6) in Ref. [23]]. The rotational energy of the core in IBO approximation is given by

$$\begin{aligned} E_{\text{rot}}^+ &= \langle \Psi_{lj}^{\text{IBO}} | H^+ | \Psi_{lj}^{\text{IBO}} \rangle = B \overline{(\hat{\mathbf{j}} - \hat{\mathbf{L}}^+ - \hat{\mathbf{S}}^+)^2} \\ &= B(j(j+1) - 2\omega^2 + \overline{(\hat{\mathbf{L}}^+ + \hat{\mathbf{S}}^+)^2}). \end{aligned} \quad (15)$$

The last two terms in this expression are again constant ones for a given core electronic state and they will be omitted below.

TABLE I. MND transformation matrix (25) for $d = 1$.

(l, j)	(l', m)								
	(0,0)	(1,-1)	(1,0)	(2,-2)	(2,-1)	(2,0)	(3,-2)	(3,-1)	(3,0)
(0,1)	0.898429	0	0.436488	0	0	0.0479734	0	0	0.00166483
(1,1)	-0.306603	0.690755	0.611348	0	0.150859	0.179158	0	0.00992159	0.0122795
(1,2)	0.306603	0.690755	-0.611348	0	0.150859	-0.179158	0	0.00992159	-0.0122795
(2,1)	0.0218707	-0.116589	-0.0782991	0.768579	0.528161	0.300986	0.0962628	0.0862089	0.0528203
(2,2)	-0.0489044	0.0869004	0.175082	0.572865	-0.393668	-0.673026	0.0717501	-0.0642563	-0.11811
(2,3)	0.0437414	0.155452	-0.156598	0.256193	-0.704215	0.601972	0.0320876	-0.114945	0.105641
(3,2)	0.00211958	-0.012386	-0.00983008	0.0856875	0.0966375	0.0626003	-0.680619	-0.604862	-0.36959
(3,3)	-0.00396538	0.00579302	0.0183904	0.0801533	-0.0451981	-0.117114	-0.63666	0.282898	0.69144
(3,4)	0.00335136	0.014688	-0.0155427	0.0406452	-0.114598	0.0989797	-0.322846	0.717278	-0.584374

Hence the total energy of the molecule in the IBO case can be recast as

$$E = \langle \Psi_{lj}^{\text{IBO}} | H | \Psi_{lj}^{\text{IBO}} \rangle = B_j(j+1) - \frac{1}{2\nu^2}, \quad (16)$$

$$\nu = n - \mu^{\text{IBO}}, \quad \mu^{\text{IBO}} = l - \tilde{l}.$$

D. Matched wave function

If the electron spends a part of time near the core and a comparable part of time far from the core, one can construct the wave function following a modified MQDT approach [27]. In the frame of this approach one chooses a certain matching radius r_M dividing the space onto two zones, the near one ($r < r_M$) and the far one ($r > r_M$). In the near zone the BO approximation is supposed to be valid; hence the wave function can be sought as a superposition of functions (4):

$$\Psi^{\text{BO}} = \sum_{l,m} C_{lm} \Psi_{lm}^{\text{BO}}. \quad (17)$$

Oppositely, in the far zone

$$\Psi^{\text{IBO}} = \sum_{l,j} C_{lj} \Psi_{lj}^{\text{IBO}}. \quad (18)$$

Thus the whole wave function is given by

$$\Psi = \begin{cases} \Psi^{\text{BO}}, & r < r_M, \\ \Psi^{\text{IBO}}, & r > r_M, \end{cases} \quad (19)$$

with the matching conditions at $r = r_M$:

$$\Psi^{\text{BO}} = \Psi^{\text{IBO}}, \quad \frac{\partial}{\partial r} \Psi^{\text{BO}} = \frac{\partial}{\partial r} \Psi^{\text{IBO}}. \quad (20)$$

Substituting (17) and (18) into (20) leads to the following system of equations for the coefficients C_{lj}, C_{lm} :

$$C_{lm} R_{lm}^{\text{BO}}(E, r_c) = \sum_{l'j} C_{l'j} R_{l'j}^{\text{IBO}}(E, r_c) \langle l'j | lm \rangle, \quad (21)$$

$$C_{lm} \frac{d}{dr} R_{lm}^{\text{BO}}(E, r_M) = \sum_{l'j} C_{l'j} \frac{d}{dr} R_{l'j}^{\text{IBO}}(E, r_M) \langle l'j | lm \rangle, \quad (22)$$

where

$$\begin{aligned} \max\{-\omega - J, -l\} &\leq m \leq \min\{-\omega + J, l\}, \\ \max\{|J - l|, \omega\} &\leq j \leq J + l, \end{aligned} \quad (23)$$

and $\langle lj | l'm \rangle$ is the transformation matrix for angular functions of BO and IBO. If a molecule is a nonpolar one [27], or if its dipole moment is small and its effect is negligible in both the near zone and the far one, then the transformation matrix can be readily obtained using Eqs. (5) and (13):

$$\langle lj | l'm \rangle = \sqrt{\frac{2j+1}{2J+1}} C_{j\omega lm}^{J\Lambda} \delta_{ll'}. \quad (24)$$

If the effect of the dipole moment is significant only in the near zone, then the transformation matrix is produced by

TABLE II. MFD transformation matrix (26) for $d = 1$.

(l, j)	(l', m)								
	(0,0)	(1,-1)	(1,0)	(2,-2)	(2,-1)	(2,0)	(3,-2)	(3,-1)	(3,0)
(0,1)	0.844439	0.101535	0.521256	-0.0148261	0.0114954	0.0674114	-0.00185693	-0.000236907	0.0023933
(1,1)	-0.419464	0.681478	0.532803	-0.263339	-0.0408562	0.0564701	-0.0329827	-0.0203233	-0.00692924
(1,2)	0.304695	0.693392	-0.604814	0.0200359	0.136857	-0.202734	0.00313573	0.00820734	-0.016084
(2,1)	-0.112386	0.12655	0.121702	0.721904	0.547642	0.34243	0.090417	0.0843642	0.0537569
(2,2)	-0.0596699	0.0632201	0.1967	0.565825	-0.404114	-0.668953	0.115273	-0.0255827	-0.0936238
(2,3)	0.0436833	0.155517	-0.156333	0.257261	-0.704767	0.600319	0.0234112	-0.111067	0.115066
(3,2)	-0.0014399	-0.00771325	0.00226048	0.1223	0.0709523	0.0194909	-0.674605	-0.607753	-0.376396
(3,3)	-0.00456297	0.00368602	0.0205328	0.0765303	-0.0357297	-0.12539	-0.635432	0.286015	0.690852
(3,4)	0.00334998	0.0146893	-0.0155354	0.0406787	-0.114612	0.0989208	-0.323323	0.717442	-0.583772

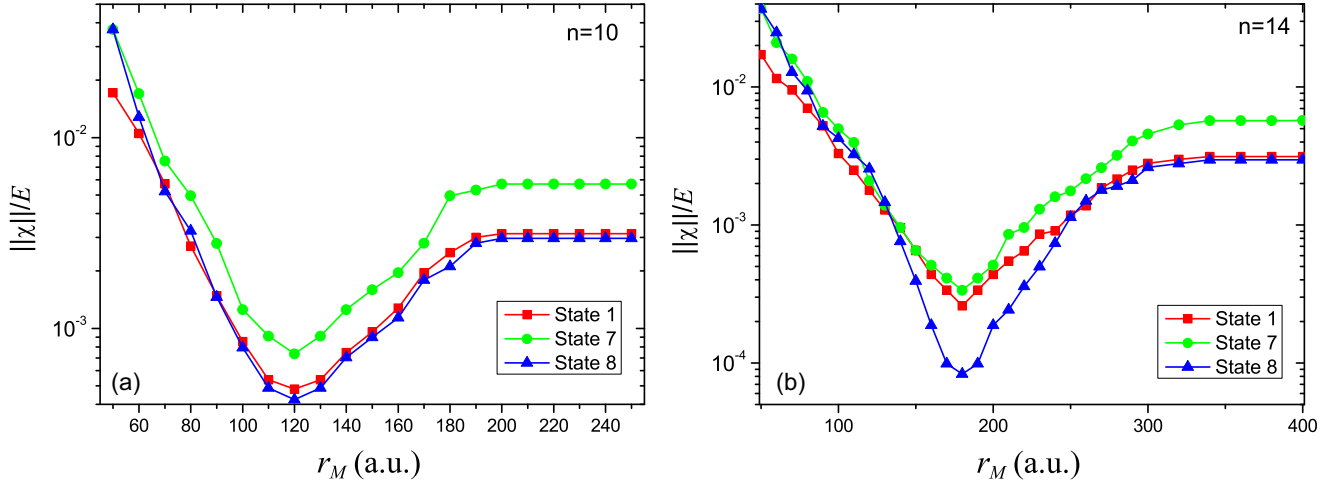


FIG. 1. (Color online) Discrepancy (27) vs matching radius for MFD wave functions. There is a pronounced minimum, corresponding to optimal value of matching radius. For $n = 10$ it is $r_M \simeq 120$ a.u. and for $n = 14$ it is $r_M \simeq 180$ a.u.

Eqs. (7) and (13):

$$\langle lj | l'm \rangle = \sqrt{\frac{2j+1}{2J+1}} a_l^{(l'm)} C_{j\omega l m}^{J\Lambda}. \quad (25)$$

The matching done with the transformation matrix (25) will be referred to below as “matching with near dipole” (MND). As an illustration, the matrix elements (25) for the dipole moment $d = 1$ are presented in Table I.

Finally, if the effect of the dipole moment is significant in both the near zone and the far one, then Eqs. (7) and (14) must be used, which yield

$$\langle lj | l'm \rangle = \sqrt{\frac{2j+1}{2J+1}} \sum_{\ell} a_{\ell}^{(lj)} a_{\ell}^{(l'm)} C_{j\omega \ell m}^{J\Lambda}, \quad (26)$$

and the corresponding matching will be referred to as “matching with far dipole” (MFD). The matrix elements (26) for the dipole moment $d = 1$ are presented in Table II. Comparing results and accuracies of MND and MFD can show significance of core dipole potential in the far zone.

The system (21) and (22) represents a homogeneous linear system on C_{lj}, C_{lm} . It has nontrivial solution when its determinant is equal to zero. This criterion provides eigenvalues of the total energy of the molecule E . Solving the system (21) and (22) for a certain E provides values of C_{lj}, C_{lm} .

E. Estimation of accuracy

Generally, the overall accuracy of a solution for the stationary Schrödinger equation with the Hamiltonian (1) is given by the value of a proper objective functional on this solution. Simplifying a bit, it can be treated as a weighted mean square error over the whole space. The proper choice of objective functional (or, in other words, of the weighting function) cannot be universal, for it is problem-specific one. For example, tunnel ionization calculations are sensitive to the wave-function accuracy in the far zone, hence more weight must be given to errors in the far zone, etc. As an example of an objective functional we take in this work the norm of the

discrepancy function:

$$\chi = (H - E)\Psi, \quad \|\chi\|^2 = \langle \chi | \chi \rangle = \int \chi^2 dV. \quad (27)$$

For the pure Born-Oppenheimer wave functions (4) one gets

$$\|\chi\|^2 = B^2 [j(j+1) - J(J+1)]^2.$$

Oppositely, for pure inverse Born-Oppenheimer wave functions (12):

$$\begin{aligned} \|\chi\|^2 &= \frac{2d^2}{v^5 \tilde{l}(\tilde{l}+1)(2\tilde{l}+2)} \sum_{\ell \ell'} a_{\ell}^{(lj)} a_{\ell'}^{(lj)} \\ &\times \sum_{\ell'', j'' \neq j} \sqrt{(2\ell+1)(2\ell'+1)} C_{\ell'0 10}^{\ell''0} C_{\ell'0 10}^{\ell''0} \\ &\times W(j1J\ell''; j''\ell) W(j1J\ell''; j''\ell') (C_{j''\omega 10}^{j\omega})^2. \end{aligned}$$

For matched wave function (19), the discrepancy (27) must be found numerically.

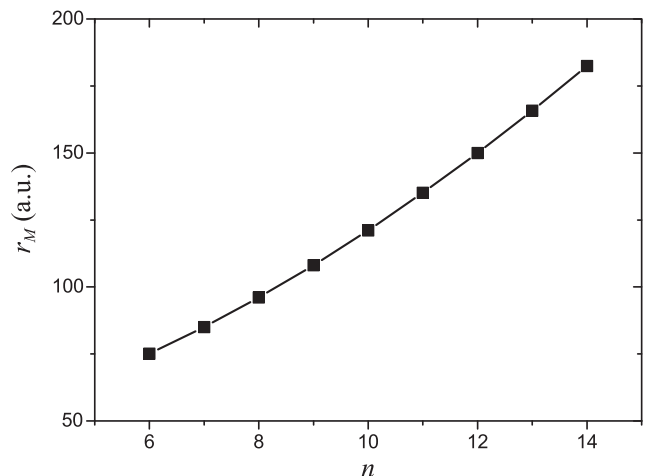


FIG. 2. Optimal matching radius r_M as the function of n .

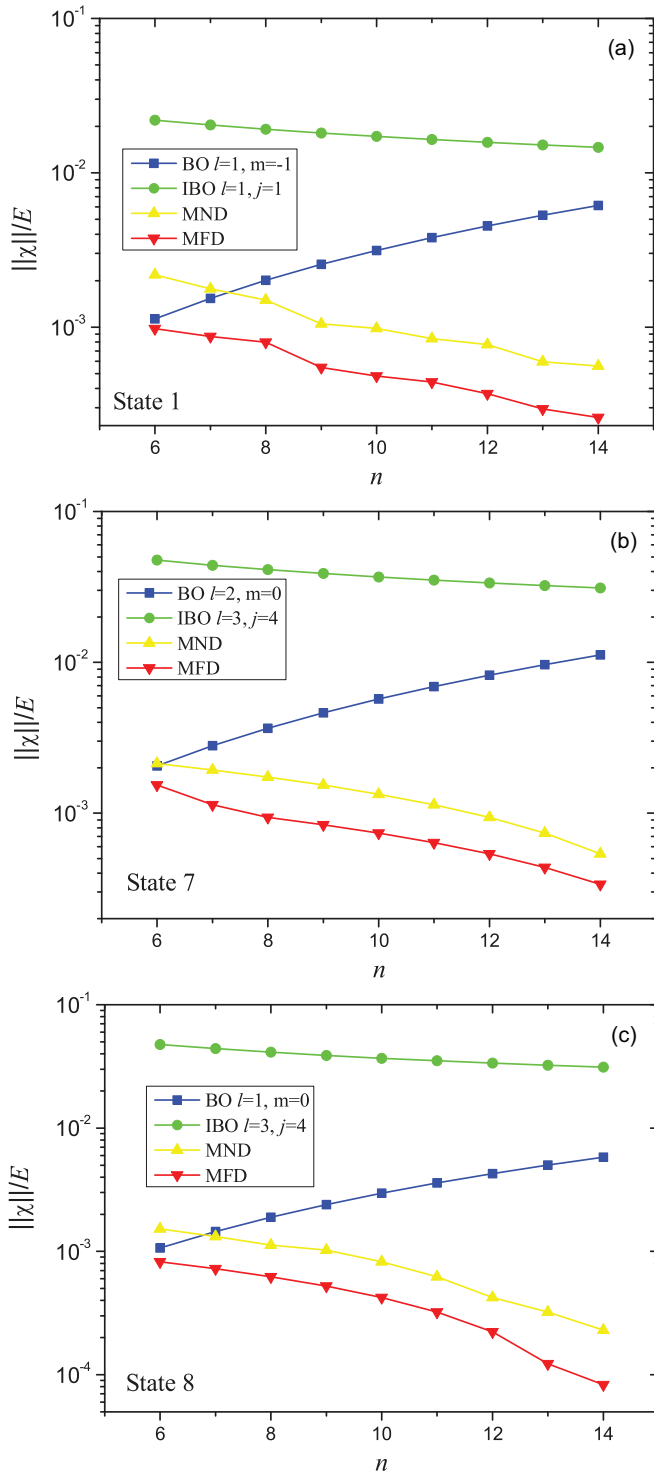


FIG. 3. (Color online) Discrepancies for states “1” (a), “7” (b), and “8” (c) as the functions of n . Blue squares: BO. Green circles: IBO. Yellow triangles: MND. Red triangles: MFD. It can be seen that best results are provided by MFD.

III. RESULTS AND DISCUSSION

For the matched wave function (19), the discrepancy (27) depends on the value of the matching radius r_M . Below we discuss this dependence. The results are presented for a sample molecule with the dipole moment $d = 1$ a.u. and the rotational

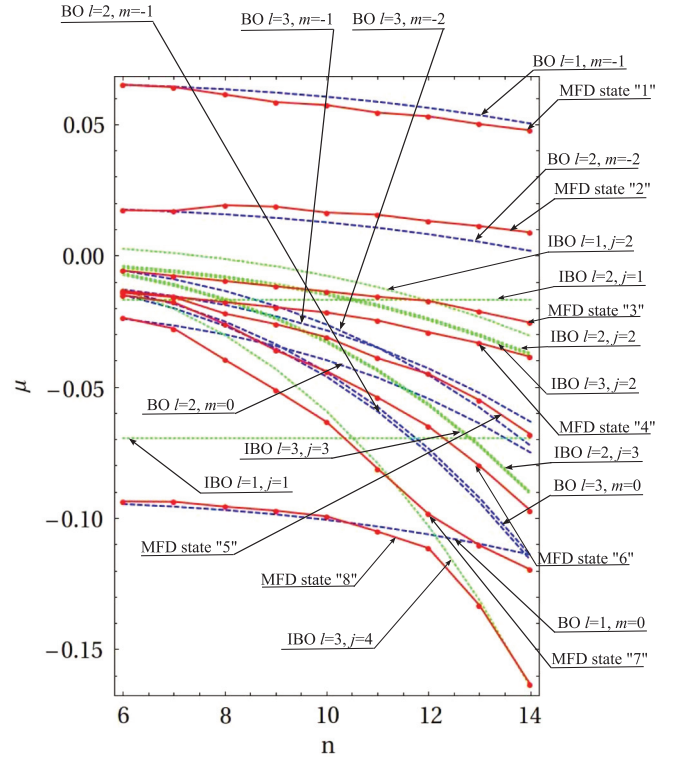


FIG. 4. (Color online) Effective quantum defects μ [see (28)] as the functions of n . Blue dashed lines: BO. Green dotted lines: IBO. Joined red points: MFD. The states from “1” to “8” are presented. The state “9” is not shown because it has constant $\mu^{\text{BO}} = -2/3$ corresponding to a pure BO case with ($l = 0, m = 0$) for all considered n . It can be seen that for $n = 6, 7, 8$ the pure BO approximation is valid for all states (state “1”: $l = 1, m = -1$; state “2”: $l = 2, m = -2$; etc.), but for $n \geq 9$ a pronounced l uncoupling takes place for most of the states, except the states “1”, “2”, and “9”. For the states “3”, “4”, “5”, and “6” the dominating contribution at $n \geq 9$ is given by the channels ($l = 2, j = 2$), ($l = 3, j = 2$), ($l = 2, j = 3$), and ($l = 3, j = 3$), respectively. The most interesting behavior is demonstrated by the states “7” and “8”, which undergo anticrossing near $n = 12$ related to crossing of BO $l = 1, m = 0$ and IBO $l = 3, j = 4$ curves.

constant $B = 3.271 \times 10^{-6}$ a.u., which corresponds to the molecule SO [38,39].

We consider a manifold of states corresponding to $\omega = 1$, $J = 1$, and $l \leq 3$. According to (23), this manifold contains nine states for each n . In the BO limit they can be labeled by l and m . Similarly, in the IBO limit they can be labeled by l and j . However, in intermediate case both these labelings become inadequate because both m and j cease to be good numbers. Therefore, we shall simply enumerate them in order of increasing energy, from state “1” to state “9”. Lest the figures below be overloaded, we present there not all these nine states but only several of them demonstrating typical behavior.

Figure 1 presents the discrepancies as the functions of r_M for the states “1”, “7”, and “8” for $n = 10$ (a) and $n = 14$ (b). It can be seen that the discrepancy can be significantly reduced by a proper choice of r_M . For $n = 10$ it is $r_M \simeq 120$ a.u. and for $n = 14$ it is $r_M \simeq 180$ a.u.

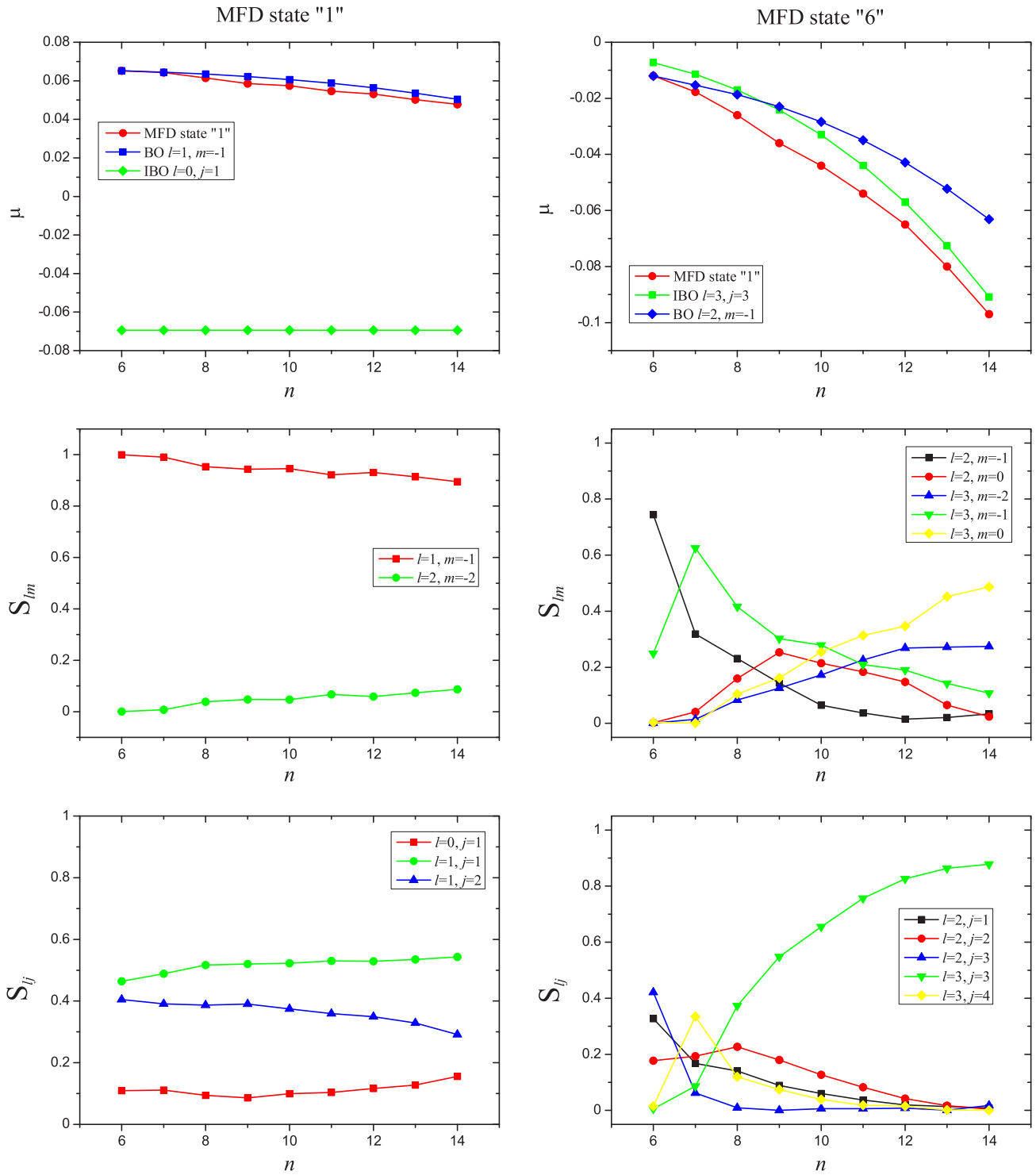


FIG. 5. (Color online) Quantum defects and partial channel contributions for the states “1” and “6”. States “1” and “6” demonstrate weak and strong l uncoupling, respectively (see comments in Results and Discussion).

Optimal r_M for other n are presented in Fig. 2.

In Fig. 3 the discrepancies are presented for states “1” (a), “7” (b), and “8” (c) as the functions of n . They are given for pure Ψ_{lm}^{BO} and pure Ψ_{lj}^{IBO} wave functions and for the matched wave functions with the proper choice of r_M (both MND and MFD). It can be seen that best results are provided by MFD.

The matched wave function (19) is a combination of several channel quantum defect functions; therefore, strictly speaking, it cannot be described by a single quantum defect value. On the other hand, it is convenient to keep a single quantum defect value for the purpose of graphic presentation of total molecule energy and its dependence on principal quantum number. We introduce here such an *ad hoc* effective quantum defect by the

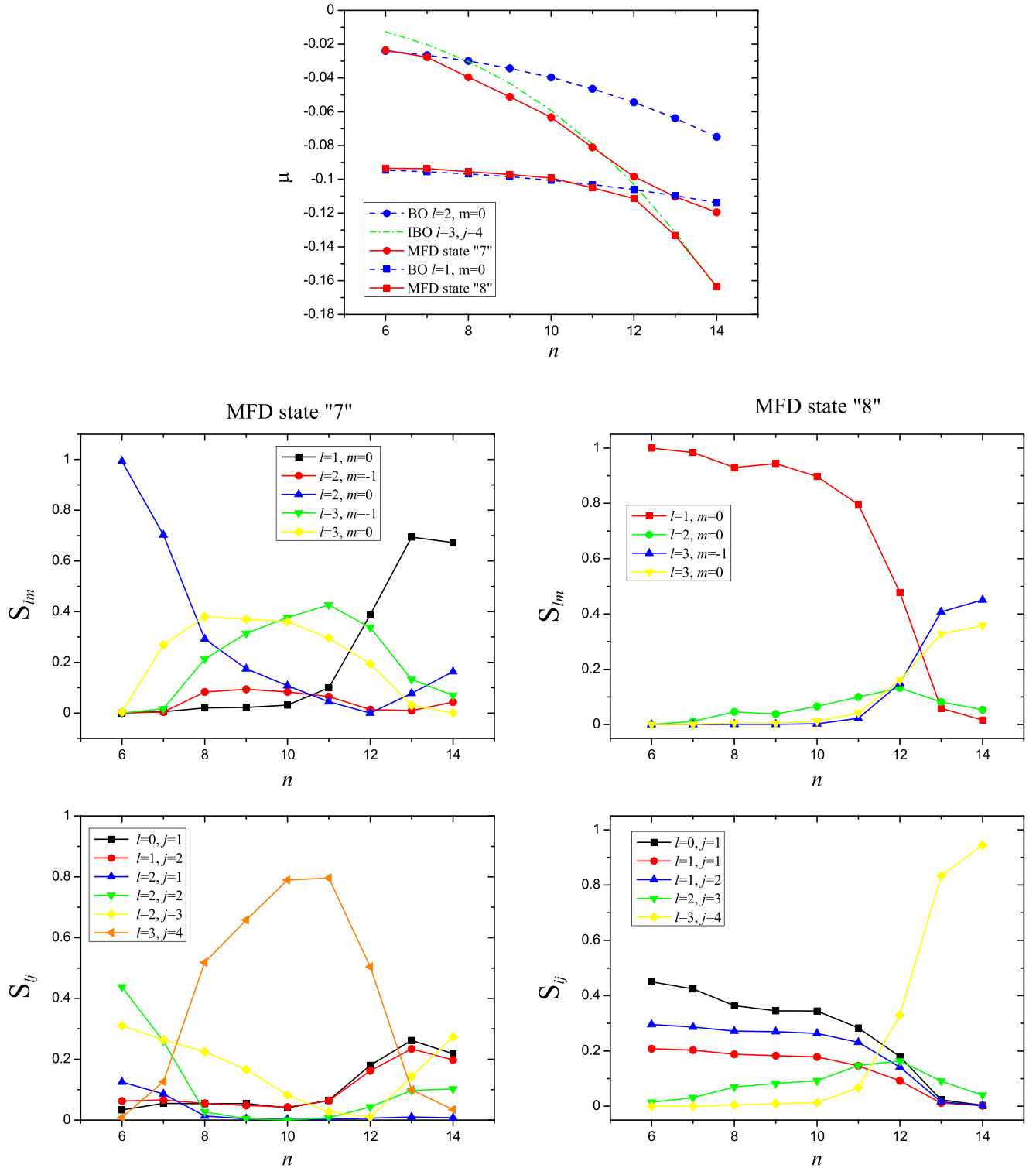


FIG. 6. (Color online) Quantum defects and partial channel contributions for the states "7" and "8". Top: quantum defects. Bottom: partial contributions for BO (S_{lm}) and IBO (S_{lj}) channels. Left: state "7". Right: state "8". Anticrossing behavior takes place near $n \simeq 12$ (see comments in Results and Discussion).

relation [it is similar to (16) with $j = 1$]

$$E = 2B - \frac{1}{2\nu^2}, \quad \nu = n - \mu. \quad (28)$$

Here, the energy E is provided by the matching procedure; hence the corresponding ν and μ can be extracted.

Figure 4 presents effective quantum defects for the states from "1" to "8" as the functions of n . Here, blue dashed lines present BO calculation [total energy E is calculated in BO approximation and effective quantum defect is extracted using (28)]; similarly, green dotted lines present IBO calculation, and joined red points present MFD calculation. The state "9" is

not presented there because it demonstrates pure BO behavior with $l = 0$, $m = 0$, and $\mu^{\text{BO}} = -2/3$. It can be seen that for $n = 6, 7, 8$ the pure BO approximation is valid for all states (state “1”: $l = 1, m = -1$; state “2”: $l = 2, m = -2$; etc.). For $n \geq 9$ pronounced l uncoupling takes place for most of the states, except the states “1”, “2”, and “9”. For the states “3”, “4”, “5”, and “6” the dominating contribution at $n \geq 9$ is given by the channels ($l = 2, j = 2$), ($l = 3, j = 2$), ($l = 2, j = 3$), and ($l = 3, j = 3$), respectively. The most interesting behavior (presented in more detail in Fig. 6) is demonstrated by the states “7” and “8”, which undergo anticrossing near $n = 12$ related to crossing of BO $l = 1, m = 0$ and IBO $l = 3, j = 4$ curves.

To evaluate relative contributions of (l, m) channels into wave function (17) and (l, j) channels into (18) we introduce weighted coefficients:

$$S_{lm} = \frac{C_{lm}^2 \int_0^{r_M} [R_{lm}^{\text{BO}}(E, r)]^2 dr}{\sum_{l'm'} C_{l'm'}^2 \int_0^{r_M} [R_{l'm'}^{\text{BO}}(E, r)]^2 dr}, \quad (29)$$

$$S_{lj} = \frac{C_{lj}^2 \int_{r_M}^{\infty} [R_{lj}^{\text{IBO}}(E, r)]^2 dr}{\sum_{l'j'} C_{l'j'}^2 \int_{r_M}^{\infty} [R_{l'j'}^{\text{IBO}}(E, r)]^2 dr}. \quad (30)$$

If BO (IBO) approximation is valid then one of coefficients S_{lm} (S_{lj}) is near to 1 and other coefficients are close to zero.

Figure 5 presents separately effective quantum defects and partial contributions for the states “1” (left) and “6” (right). State “1” demonstrates relatively large quantum defect $\mu^{\text{BO}} \simeq 0.06$ in the BO limit. Correspondingly, l coupling is dominating, and l uncoupling is relatively weak. Therefore, the quantum defect of the state “1” remains nearly constant. This interpretation is confirmed by the graphs of partial contributions for BO and IBO channels (S_{lm} and S_{lj} , respectively): one BO channel, namely the channel ($l = 1, m = -1$), gives the main contribution into the wave function. Oppositely, the state “6” demonstrates small quantum defect $\mu^{\text{IBO}} \simeq 0.009$ in the IBO limit; hence there is strong l uncoupling starting from $n = 9$. Correspondingly, one IBO channel ($l = 3, j = 3$) rapidly becomes dominating, and the quantum defect approaches the IBO curve defined by relation (28) with $j = 3$ and very small $\mu^{\text{IBO}} \simeq -0.0002$, which gives $\mu \simeq -n^3 B[j(j+1) - 2] = -10n^3 B$.

Figure 6 presents the states “7” and “8”. For $n \leq 8$ they both demonstrate the BO picture: each one is dominated by one BO channel and quantum defects are close to pure BO values. The state “7” has lesser quantum defect ($\mu^{\text{BO}} \simeq 0.019$) in the BO limit; therefore, it significantly l uncouples at $9 \leq n \leq 11$, IBO channel ($l = 3, j = 4$) becomes dominating, and quantum defect approaches corresponding IBO value (28), where $\mu^{\text{IBO}} \ll 1$; hence $\mu \simeq -n^3 B[j(j+1) - 2] = -18n^3 B$. The state “8” has greater quantum defect in the BO limit; therefore, its l uncoupling is weak, and its quantum defect remains nearly constant up to $n = 11$. Further, as noted above, the states “7” and “8” demonstrate anticrossing near $n = 12$. This anticrossing is reflected also in the behavior of channel contributions. These contributions are presented in the lower part of Fig. 6, on the left side for the state “7” and on the right side for the state “8”. One can see that immediately before anticrossing the main contribution into the state “7” is from

the IBO channel ($l = 3, j = 4$), and the main contribution into the state “8” is from the BO channel ($l = 1, m = 0$), whereas immediately after the anticrossing the distribution of dominating channels is reversed: main contribution into “7” is from BO ($l = 1, m = 0$) and the one into “8” is from IBO ($l = 3, j = 4$). This anticrossing can be interpreted in classical mechanics’ terms as a resonance between rotation of the core and the precession of the Rydberg electron’s orbit [36].

IV. CONCLUSION

We have developed a generalized MQDT technique for calculating spectra and wave functions of nonpenetrating RS in polar molecules, consistently taking into account l uncoupling for the Rydberg electron due to the core rotation as well as l coupling due to nonsphericity of the core dipole potential. The results are presented for the case of SO molecule. They show that the effect of the core dipole potential cannot be neglected even at very far distances from the core (i.e., in IBO zone).

The next steps in developing an outlined approach can include (i) short-range interactions of the outer electron with the core (thus extending the approach on penetrating RS also), (ii) electron-vibrational mixing, (iii) spin effects, involving both electron and nuclear spins, (iv) perturbation of the core Λ doublets due to their interaction with the Rydberg electron [40], etc. There are also left to be investigated spectra and wave functions in ionization and dissociation continua. This can be done mainly along the lines of works [14,15,28] with the effect of the core dipole potential in the far IBO zone properly accounted for.

The developed technique can be useful in theoretical description of any phenomena involving RS of polar molecules and in calculations of corresponding molecular characteristics. It seems particularly appropriate in cases where precision of wave function in the far zone is essential, such as calculations of oscillator forces and cross sections of tunnel ionization.

ACKNOWLEDGMENT

The authors thank Dr. V. E. Chernov for interest in the work and fruitful discussions.

APPENDIX: COULOMB FUNCTIONS

For an electron with energy $E = -1/(2v^2) < 0$ in Coulomb-dipole potential the radial Schrödinger equation in atomic units can be written as

$$\left(\frac{d^2}{dr^2} - \frac{\tilde{l}(\tilde{l}+1)}{r^2} + \frac{2}{r} - \frac{1}{v^2} \right) y = 0. \quad (A1)$$

For noninteger \tilde{l} this equation has two linearly independent solutions [25]:

$$f = \frac{v^{\tilde{l}+1}}{\Gamma(2\tilde{l}+2)} M_{v, \tilde{l}+1/2} \left(\frac{2r}{v} \right), \quad (A2)$$

$$y_2 = \frac{v^{-\tilde{l}}}{\Gamma(-2\tilde{l})} M_{v, -\tilde{l}-1/2} \left(\frac{2r}{v} \right), \quad (A3)$$

where $M_{\nu,\rho}$ is the Whittaker function [41]. However, for integer \tilde{l} these two functions become dependent; hence y_2 must be replaced by

$$y_3 = \frac{f A(\nu, \tilde{l}) \cos \pi(2\tilde{l} + 1) - y_2}{\sin \pi(2\tilde{l} + 1)}, \quad (\text{A4})$$

where

$$A(\nu, \tilde{l}) = \frac{\Gamma(\nu + \tilde{l} + 1)}{\nu^{2\tilde{l}+1} \Gamma(\nu - \tilde{l})}. \quad (\text{A5})$$

The functions f and y_3 are linearly independent for all \tilde{l} , both integer and noninteger ones. Following Seaton [25] we also

introduce the functions

$$s = \sqrt{\frac{A(\nu, \tilde{l})}{2}} f, \quad c = -\sqrt{\frac{1}{2A(\nu, \tilde{l})}} y_3, \quad (\text{A6})$$

which satisfy the simple asymptotic relation

$$\lim_{r \rightarrow \infty} \frac{s}{c} \rightarrow \tan \pi(\nu - \tilde{l}), \quad (\text{A7})$$

and finally construct the radial functions used in Eqs. (4) and (12):

$$R^{\text{BO}} = s, \quad R^{\text{IBO}} = s - \tan \pi(\nu - \tilde{l})c. \quad (\text{A8})$$

-
- [1] M. B. Bell, L. W. Avery, E. R. Seaquist, and J. P. Vallée, *Publ. Astron. Soc. Pac.* **112**, 1236 (2000).
- [2] M. B. Bell, L. W. Avery, J. M. MacLeod, and J. P. Vallée, *Astrophys. Space Sci.* **333**, 377 (2011).
- [3] M. B. Bell, *Astrophys. Space Sci.* **340**, 127 (2012).
- [4] S. Yoshida, C. O. Reinhold, J. Burgdörfer, S. Ye, and F. B. Dunning, *Phys. Rev. A* **86**, 043415 (2012).
- [5] D. Jaksch, J. I. Cirac, P. Zoller, S. L. Rolston, R. Côté, and M. D. Lukin, *Phys. Rev. Lett.* **85**, 2208 (2000).
- [6] I. E. Protsenko, G. Reymond, N. Schlosser, and P. Grangier, *Phys. Rev. A* **65**, 052301 (2002).
- [7] D. Tong, S. M. Farooqi, J. Stanojevic, S. Krishnan, Y. P. Zhang, R. Côté, E. E. Eyler, and P. L. Gould, *Phys. Rev. Lett.* **93**, 063001 (2004).
- [8] M. Viteau, M. G. Bason, J. Radogostowicz, N. Malossi, D. Ciampini, O. Morsch, and E. Arimondo, *Phys. Rev. Lett.* **107**, 060402 (2011).
- [9] J. Honer, R. Löw, H. Weimer, T. Pfau, and H. P. Büchler, *Phys. Rev. Lett.* **107**, 093601 (2011).
- [10] A. V. Gorshkov, J. Otterbach, M. Fleischhauer, T. Pohl, and M. D. Lukin, *Phys. Rev. Lett.* **107**, 133602 (2011).
- [11] T. Peyronel, *Nature (London)* **488**, 57 (2012).
- [12] T. E. Lee, H. Häffner, and M. C. Cross, *Phys. Rev. Lett.* **108**, 023602 (2012).
- [13] J. D. Pritchard, C. S. Adams, and K. Mølmer, *Phys. Rev. Lett.* **108**, 043601 (2012).
- [14] M. Arif, C. Jungen, and A. L. Roche, *J. Chem. Phys.* **106**, 4102 (1997).
- [15] C. Jungen and A. L. Roche, *Can. J. Phys.* **79**, 287 (2001).
- [16] J. A. Keele, M. E. Hanni, S. L. Woods, S. R. Lundeen, and C. W. Fehrenbach, *Phys. Rev. A* **83**, 062501 (2011).
- [17] J. A. Keele, C. S. Smith, S. R. Lundeen, and C. W. Fehrenbach, *Phys. Rev. A* **88**, 022502 (2013).
- [18] S. Civis, M. Ferus, V. E. Chernov, and E. M. Zanozina, *Astron. Astrophys.* **554**, A24 (2013).
- [19] S. Civis, M. Ferus, P. Kubelik, V. E. Chernov, and E. M. Zanozina, *Astron. Astrophys.* **545**, A61 (2012).
- [20] S. Civis, M. Ferus, P. Kubelik, P. Jelinek, and V. E. Chernov, *Astron. Astrophys.* **541**, A125 (2012).
- [21] B. A. Zon, *Sov. Phys. JETP* **75**, 19 (1992).
- [22] J. K. G. Watson, *Mol. Phys.* **81**, 227 (1994).
- [23] B. A. Zon, *Phys. Lett. A* **203**, 373 (1995).
- [24] D. L. Dorofeev, S. V. Elfimov, and B. A. Zon, *Phys. Rev. A* **85**, 022509 (2012).
- [25] M. J. Seaton, *Proc. Phys. Soc. (London)* **88**, 801 (1966).
- [26] M. J. Seaton, *Proc. Phys. Soc. (London)* **88**, 815 (1966).
- [27] U. Fano, *Phys. Rev. A* **2**, 353 (1970).
- [28] J. J. Kay *et al.*, *J. Chem. Phys.* **134**, 114313 (2011).
- [29] S. Raouafi, G.-H. Jeung, and C. Jungen, *J. Mol. Spectrosc.* **196**, 248 (1999).
- [30] Z. J. Jakubek and R. W. Field, *Phys. Rev. Lett.* **72**, 2167 (1994).
- [31] Z. J. Jakubek and R. W. Field, *J. Mol. Spectrosc.* **179**, 99 (1996).
- [32] Z. J. Jakubek and R. W. Field, *Philos. Trans. R. Soc. London A* **355**, 1507 (1997).
- [33] Z. J. Jakubek and R. W. Field, *J. Mol. Spectrosc.* **205**, 197 (2001).
- [34] J. Li *et al.*, *J. Mol. Spectrosc.* **193**, 403 (1999).
- [35] J. O. Clevenger, N. A. Harris, R. W. Field, and J. Li, *J. Mol. Spectrosc.* **193**, 412 (1999).
- [36] J. J. Kay, S. N. Altunata, S. L. Coy, and R. W. Field, *Mol. Phys.* **105**, 1661 (2007).
- [37] L. D. Landau and E. M. Lifshitz, *Quantum Mechanics, Nonrelativistic Theory* (Pergamon, New York, 1991).
- [38] S. Midda and A. K. Dasa, *Eur. Phys. J. D* **27**, 109 (2003).
- [39] NIST, <http://webbook.nist.gov/chemistry/>
- [40] D. L. Dorofeev and B. A. Zon, *JETP* **83**, 485 (1996).
- [41] E. T. Whittaker and G. N. Watson, *A Course of Modern Analysis*, 4th ed. (Cambridge University Press, Cambridge, UK, 1927) (reissued 1996).